Classification of the vegetated terrain using polarimetric SAR processing techniques

Sang-Eun Park[1] and Wooil M. Moon[1,2]
1. School of Earth & Environmental Sciences (SEES), Kwan-ak Gu Shil-rim dong san 56-1, Seoul National University, Seoul 151-742, Korea (separk@eos1.snu.ac.kr , wmoon@eos1.snu.ac.kr)
2. Geophysics, University of Manitoba, Winnipeg, MB R3T 2N2 Canada (wmoon@cc.umanitoba.ca)

Abstract: Classification of Earth natural components within a full polarimetric SAR image is one of the most important applications of radar polarimetry in remote sensing. In this paper, the unsupervised classification algorithms based on the combined use of the polarimetric processing technique such as the target decomposition and statistical complex Wishart classification method are evaluated and applied to vegetated terrain in Jeju volcanic island.

1. Introduction

Polarimetric SAR (Synthetic Aperture Radar) data help researchers understand and quantify the scattering properties of natural scenes and their variability under different conditions better than single polarization SAR data. Terrain classification is an important polarimetric SAR application. Recently polarimetric SAR image classification approaches have been focused on the combined use of the inherent characteristics of polarimetric SAR data and its physical scattering mechanisms [1-3]. Lee et al. [1] and Pottier and Lee [2] have applied eigenvector-based target decomposition to initially segment the data, followed by iterated refined classification based on the Complex Wishart classifier. In 2004, Lee et al. [3] developed another unsupervised classification algorithm based on the model-based target decomposition and the statistical Wishart classifier.

In this paper, we discuss the application of recent advancements in polarimetric processing techniques to a classification of the vegetated terrain. The land cover discrimination characteristics in the 'eigenvector-based decomposition and Wishart classifier' and the 'model-based decomposition and Wishart classifier' are studied. Theses classification techniques are applied to fully polarimetric NASA/JPL AIRSAR data in Jeju volcanic island.

2. Method of Radar Target Decomposition

For incoherent scattering, the polarimetric coherency and covariance matrices are useful to describe terrain physical properties. Following the target decomposition theorem, fully-polarimetric covariance and coherency matrices can be decomposed into a weighted sum of simpler matrices.

1) Eigenvector-based decomposition

The coherency matrix $[T]$ can be decomposed into real eigenvalues and orthogonal eigenvectors [4-5];

$$[T]=[U_3][\Sigma][U_3]^{-1}=\sum_{i=1}^{3}\lambda_i \vec{e}_i \cdot \vec{e}_i^{+} \qquad (1)$$

where $[\Sigma]$ is a 3×3 diagonal matrix with real eigenvalues and $[U_3]=[\vec{e}_1 \quad \vec{e}_2 \quad \vec{e}_3]$ is a unitary matrix with the three orthogonal eigenvectors. The polarimetric entropy is defined as

$$H=-\sum_{i=1}^{3}P_i \log_3(P_i) \quad P_i=\lambda_i/(\lambda_1+\lambda_2+\lambda_3). \qquad (2)$$

Each eigenvector can be expressed in terms of five angles

$$\vec{e}_i=\left[\cos\alpha_i \quad \sin\alpha_i\cos\beta_i e^{(j\delta_i)} \quad \sin\alpha_i \sin\beta_i e^{(j\gamma_i)}\right]^T. \qquad (3)$$

By using a three symbol Bernoulli process, average scattering mechanism $\bar{\alpha}$ is defined as

$$\bar{\alpha}=\sum_{i=1}^{3}P_i\alpha_i=P_1\alpha_1+P_2\alpha_2+P_3\alpha_3. \qquad (4)$$

In general, $\bar{\alpha}$ reveals the averaged scattering mechanism ranging from 0° to 90°, and the polarimetric entropy is a useful scalar descriptor of the randomness of the scattering process with range $0 \le H \le 1$. Based on the $H/\bar{\alpha}$ plane, the random scattering mechanisms can be characterized into eight basic cases (Fig. 1).

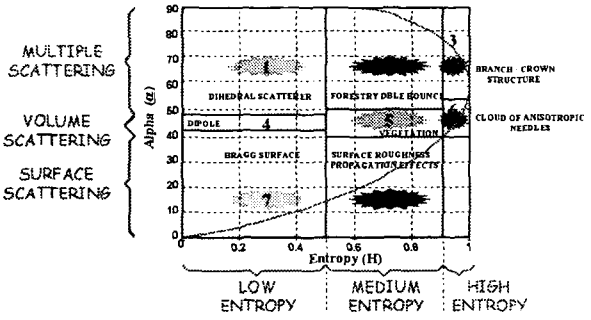

Fig. 1. H/α plane for polarimetric SAR classification.

2) Model-based decomposition

In the reflection symmetric case, the covariance matrix $[C]$ can be decomposed into three simple physical scattering models [6].

$$[C]=\begin{bmatrix} f_S|b|^2+f_D|a|^2+f_V & 0 & f_Sb+f_Da+f_V/3 \\ 0 & 2f_V/3 & 0 \\ f_Sb+f_Da^*+f_V/3 & 0 & f_S+f_D+f_V \end{bmatrix} \quad (5)$$

where f_S, f_D, and f_V are the surface, double-bounce, and volume scatter contributions to the backscatter at VV polarization. Consequently, the scattering contribution of each scattering mechanism to the span P is defined as

$$P=\langle|S_{HH}|^2\rangle+2\langle|S_{HV}|^2\rangle+\langle|S_{VV}|^2\rangle=P_S+P_D+P_V \quad (6)$$

with $P_S=f_S(1+|b|^2)$, $P_D=f_D(1+|a|^2)$, and $P_V=8f_V/3$. Following model-based target decomposition, each pixel can be labeled by the dominant scattering mechanism as on of three scattering categories: surface (S), double-bounce (D), and volume (V) scattering (Fig. 2).

3. Unsupervised classification algorithm

Image classification results of the target decomposition methods can be significantly improved by iterated refinement using the complex Wishart classifier [1-3]. The multi-look polarimetric covariance and coherency matrices have the complex Wishart distribution [7]. The initial segmentation map based on the decomposition technique defines training sets for classification based on the Wishart distribution. Applying the maximum-likelihood classifier to the Wishart distribution, a distance measure between a sample covariance or coherency matrix Z and a cluster mean V_m of the m^{th} class is

$$d(Z,V_m)=\ln|V_m|+Tr(V_m^{-1}Z). \quad (7)$$

The pixel is assigned the class with the minimum distance. Mathematically, the pixel is assigned to class ω_m, if

$$d(Z,V_m)<d(Z,V_j) \text{ for all } j\neq m. \quad (8)$$

Figure 3 shows the actual implementation procedures of the eigenvector-based decomposition and Wishart (HA-Wishart) classifier and the model-based decomposition and Wishart (FD-Wishart) classifier.

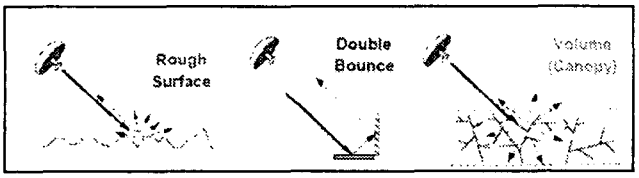

Fig. 2. Schematics of three simple scattering mechanisms used in the model-based decomposition.

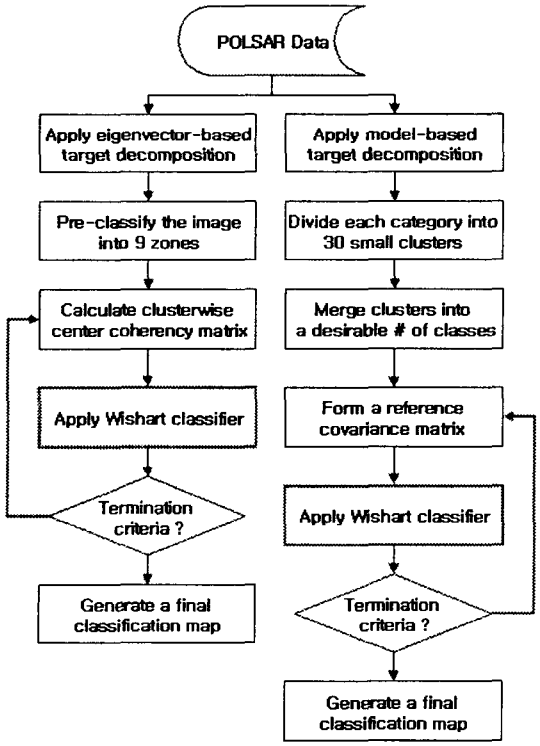

Fig. 3. Flowchart of the HA-Wishart classification (left) and the FD-Wishart classification (right) algorithms.

4. Experimental Results

The study site selected is located in the middle-eastern part of the Jeju-island, Korea as shown in Fig. 4. The study area mostly comprises grassy field pruned to pasture animals or secure arable areas. Land use pattern of this grassy area are fragile and sophisticated due to the rapid development. The polarimetric SAR data used here is the NASA/JPL AIRSAR data which are acquired during the PACRIM-II Korea campaign on September 30, 2000. In this research L-band (with center frequencies at 1.26 GHz) fully polarimetric SAR data is processed to mapping land cover. To improve class definition the statistical variation in stochastic data, we apply the polarimetry preserving speckle filter [8].

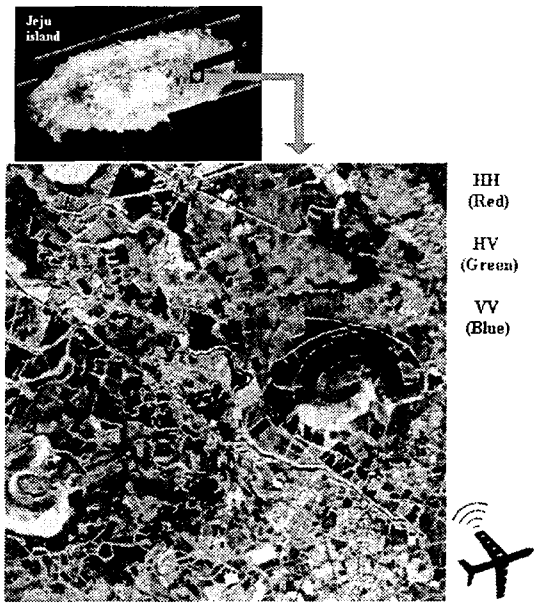

Fig. 4. L-band AIRSAR image of the study area.

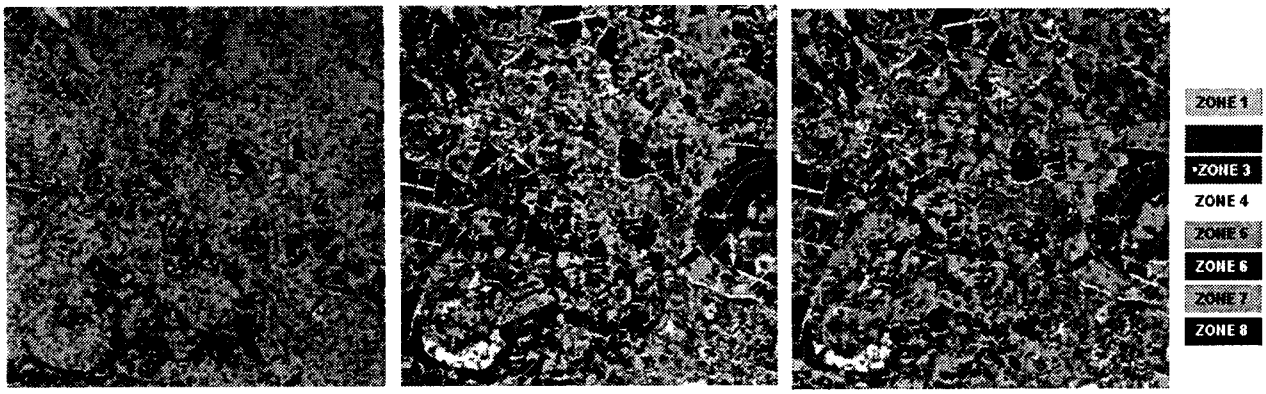

(a) Original H/alpha classification (b) After 2nd iteration (c) After 4th iteration

Fig. 5. HA-Wishart Classification

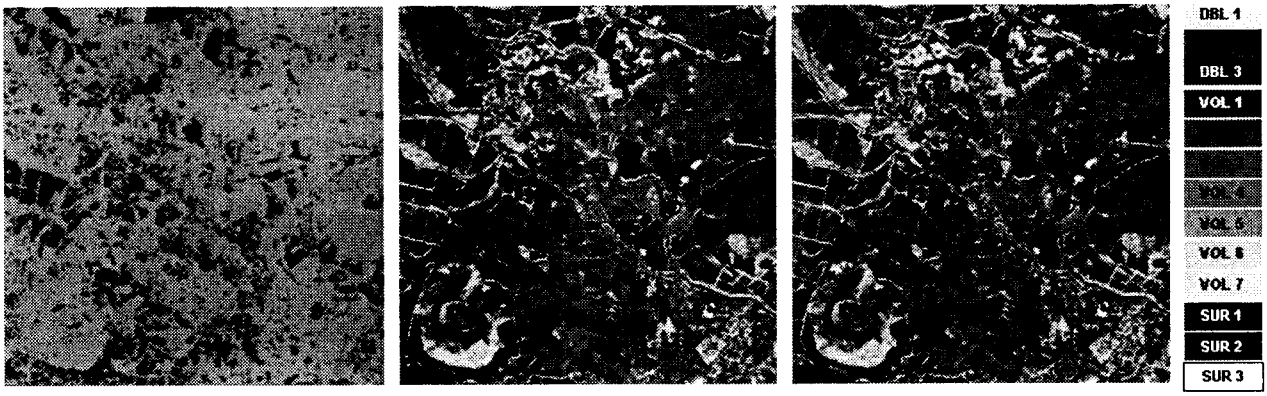

(a) Original model-based scattering category (b) After 2nd iteration (c) After 4th iteration

Fig. 6. FD-Wishart Classification

Figure 5 and 6 show the unsupervised classification results using the HA-Wishart and the FD-Wishart classifier, respectively. Significant improvement in classification of details during iterations can be observed. In the FD-Wishart classifier, we have seven classes with volume scattering because the large vegetation area in the image as shown in Fig. 6.

Figure 7 and 8 show the vegetation type discrimination characteristics in the HA-Wishart classifier and the FD-Wishart classifier, respectively. A pasture and growing crops are well distinguishable from the natural grassland and forestry using unsupervised polarimetric SAR classification at L-band frequency. The FD-Wishart classifier shows better discrimination ability between the forestry and natural grassland than the HA-Wishart classifier. However, mature crops and natural grasses are more distinguishable in the HA-Wishart classifier.

5. Conclusion

The unsupervised classification algorithms based on the combined use of the polarimetric processing technique such as the target decomposition and statistical complex Wishart classification method are evaluated and applied to vegetated terrain in Jeju volcanic island. Two types of the target decomposition methods are used to initially classify the polarimetric SAR image. One is the eigenvector-based decomposition of the coherency matrix and the other is the

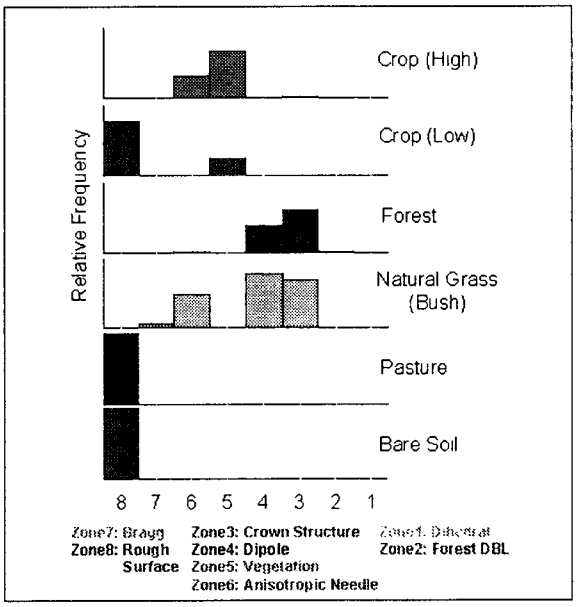

Fig. 7. Cluster-wise vegetation discrimination analysis of the HA-Wishart Classier

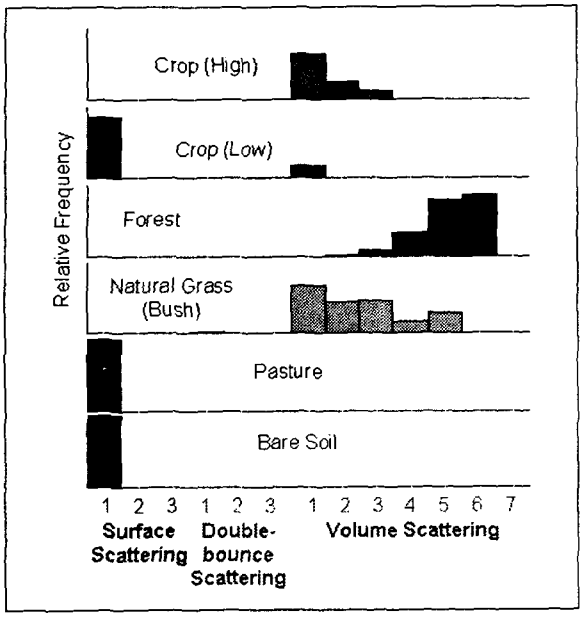

Fig. 8. Cluster-wise vegetation discrimination analysis of the FD-Wishart Classier

model-based covariance matrix decomposition. As an experimental result, the FD-Wishart classifier is more stable in convergence than the HA-Wishart classifier. Since the convergence in unsupervised classification algorithms depends on the initial seeding of candidate classes, the cluster merging step should be carefully implemented in the FD-Wishart classification algorithm.

Acknowledgment

This research is funded by the SEES (BK21), Seoul National University, and NSERC of Canada grant (A-7400) to W. M. Moon.

References

[1] Lee J.S., M. R. Grunes, T. L. Ainsworth, L. J. Du, D. L. Schuler, and S. R. Cloude, 1999. Unsupervised classification using polarimetric decomposition and the complex Wishart classifier, *IEEE Trans. Geosci. Remote Sensing*, 37(5), pp. 2249-2258.

[2] Pottier, E and J.S. Lee, 2000. Unsupervised classification scheme of PolSAR images based on the complex Wishart distribution and the H/A/Alpha – Polarimetric decomposition theorem, *Proc. EUSAR 2000*, Munich, Allemagne. 23-25 May 2000.

[3] Lee J.S., M. R. Grunes, E. Pottier, amd L. Ferro-Famil, 2004. Unsupervised terrain classification preserving polarimetric scattering characteristics, *IEEE Trans. Geosci. Remote Sensing*, 42(4), pp. 722-731.

[4] Cloude S. R., and E. Pottier, 1996. A review of target decomposition theorems in radar polarimetry, *IEEE Trans. Geosci. Remote Sensing*, 34(2), pp. 498-518.

[5] Cloude S. R., and E. Pottier, 1997. An Entropy based classification scheme for land applications of polarimetric SAR, *IEEE Trans. Geosci. Remote Sensing*, 35(1), pp. 68-78.

[6] Freeman A., and S. L. Durden, 1998. A three-component scattering model for polarimetric SAR data, *IEEE Trans. Geosci. Remote Sensing*, 36(3), pp. 963-973.

[7] Lee, J. S., M. R. Grunes, and R. Kwok, 1994. Classification of multi-look polarimetric SAR imagery based on complex Wishart distribution, *Int. J. Remote Sens.*, 15(11), pp. 2299–2311.

[8] Lee J. S., R. W. Jansen, M. R. Grunes, and G. Grandi, 1999. Polarimetric SAR speckle Filtering and its implication for classification, *IEEE Trans. Geosci. Remote Sensing*, 37(5), pp. 2363-2373.